Materials Science and Engineering B 119 (2005) 119–124

www.elsevier.com/locate/mseb

Combustion synthesis and characterization of Sn^{4+} substituted nanocrystalline $NiFe_2O_4$

S. Balaji [a], R. Kalai Selvan [b], L. John Berchmans [b], S. Angappan [b], K. Subramanian [a], C.O. Augustin [b,*]

[a] *Department of Physics, Thiagarajar College of Engineering, Madurai 625015, India*
[b] *Central Electrochemical Research Institute, Karaikudi 630006, India*

Received 19 February 2004; received in revised form 21 January 2005; accepted 21 January 2005

Abstract

A series of Sn^{4+} substituted $NiFe_2O_4$ with general formula $Ni_{1-x}Sn_xFe_2O_4$ ($x = 0.0$, 0.2, 0.4, 0.6, and 0.8) has been prepared by novel combustion synthetic method. The prepared compounds have been sintered at 1000 °C and evaluated for their structural and electrical properties. XRD studies reveal the synthesized compounds are nanocrystalline size with cubic structure. The Fourier transform infrared (FT-IR) spectra show the characteristic features of the synthesized ferrite compounds. The UV–vis spectra reveal the optical band gap of the synthesized compounds. The dc electrical conductivity of the compounds found to increase with increasing measuring temperature. A maximum dc electrical conductivity of 6.0 S cm^{-1} was obtained at a measuring temperature of 1000 °C in the composition of $x = 0.8$, for which the activation energy for conduction is found to be minimum.

Keywords: Nanocrystallines; Sn–Ni ferrites; X-ray spectroscopy; Electrical measurements

1. Introduction

Spinels of general formula AB_2O_4 are known to be technologically important materials because of their tailorable properties to meet stringent requirements in various applications [1,2]. Especially ferrites belonging to this class of materials are gaining prominence owing to their efficacious properties such as high thermodynamic stability, high electrical conductivity, and high corrosion resistance, making them suitable in metallurgical field and other high temperature areas. Nickel ferrite and its derivatives have been tried as inert anodes for electrometallurgical applications particularly for the production of aluminum using Hall–Heroult process [3,4]. Earlier studies have been made to evaluate structural, electrical,and morphological features of $NiFe_2O_4$ synthesized by various methods [5,6]. It has been reported that the substitution on A-site or B-site of this compound improves its overall properties. The substitution has been tried to synthesize different compositions of ferrites such as Ni–Zn [7], Ni–Pb [8], Ni–Cu [9], Ni–Al [10], Ni–Mn [11], Ni–Gd [12], Ni–Mg [13], and Ni–Co [14]. The magnetic studies on Sn substituted nickel ferrite have been reported in detail [15]. The conventional way of preparing the ferrite is by solid-state reaction, which involves the mixing of oxides with intermittent grinding followed by high temperature sintering between 1300 and 1700 °C. Though the process remains simple it has several drawbacks such as high reaction temperature, larger particle size, limited degree of homogeneity, and low sinterability. On the other hand, the wet chemical processes such as sol–gel, co-precipitation, citrate-gel and combustion synthesis method yield sub-micron sized particles with good homogeneity, high sinterability, and good control of stoichiometry [16]. Further the combustion synthetic route is preferred, because of its potential advantages such as low processing time, low external energy consumption, self-sustaining instantaneous reaction, and high yield of nanosized particles.

* Corresponding author. Fax: +91 4565 227713/227779.
E-mail address: caugustin@rediffmail.com (C.O. Augustin).

0921-5107/$ – see front matter © 2005 Elsevier B.V. All rights reserved.
doi:10.1016/j.mseb.2005.01.021

The present work envisages the substitution of Sn^{4+} in $NiFe_2O_4$ to ameliorate the electrical and structural properties of $NiFe_2O_4$ to make it more suitable, for anode material in molten salt systems and in high temperature applications. This paper highlights the structural characterization of the samples by X-ray diffraction, Fourier transform infrared (FT-IR) spectroscopy to identify the stretching and bending frequencies of octahedral and tetrahedral occupants and UV–vis spectroscopy for optical band gap calculations. The dc electrical conductivities of the synthesized materials were measured by modified four-probe method.

2. Experimental

The nanocrystalline $Ni_{1-x}Sn_xFe_2O_4$ ($x = 0.0$, 0.2, 0.4, 0.6, and 0.8) was prepared by novel combustion method [17]. Stoichiometric quantities of analytical grade $Ni(NO_3)_2{\cdot}6H_2O$, $Fe(NO_3)_3{\cdot}9H_2O$, $SnCl_2{\cdot}2H_2O$ were taken as cation precursors and were dissolved in minimum quantity of triple distilled water. The required quantity of urea was also added to the solution. The reactants were allowed to boil on a heater at 300 °C, to initiate a self-propagating exothermic reaction evolving large amounts of gases. The gas evolution was followed by frothing and swelling of the resultant product, which finally ruptured to yield the foamy powder of $Ni_{1-x}Sn_xFe_2O_4$ ($x = 0.0$, 0.2, 0.4, 0.6, and 0.8). The decomposition reactions of starting compounds are:

$$Ni(NO_3)_2 \cdot 6H_2O \Rightarrow NiO + NO_2 + NO + 6H_2O \quad (1)$$

$$Fe(NO_3)_3 \cdot 9H_2O \Rightarrow 0.33Fe_3O_4 + 9H_2O + 1.5NO + 1.5NO_2 + 1.6O_2 \quad (2)$$

$$CO(NH_2)_2 + 1.5O_2 \Rightarrow CO_2 + 2H_2O + N_2 \quad (3)$$

From the above reactions it has been understood that the decomposition of urea is highly exothermic over other starting compounds aiding the decomposition of nitrate salts into desired product at faster rate with low external energy consumption. Hence, urea is identified to be more suited organic fuel over other fuels. The overall reaction becomes:

$$(1-x)Ni(NO_3)_2 \cdot 6H_2O + 2Fe(NO_3)_3 \cdot 9H_2O + xSnCl_2 \cdot 2H_2O + CO(NH_2)_2 \Rightarrow Ni_{1-x}Sn_xFe_2O_4 + 2HCl + (15-4x)H_2O + (5-x)N_2 + (9.5-3x)O_2 + CO_2 \quad (4)$$

The synthesized powders were compacted under a pressure of 3.5 tonnes cm^{-2} to get dense pellets. The pellets were subjected to sintering at 1000 °C for 60 h in air in a resistance furnace to impart the mechanical strength of the compounds. The structural homogeneity, crystal structure, phase formation, crystalline size were determined from XRD patterns using Cu Kα ($\alpha = 1.5418$ Å) radiation with 2θ value ranges from 10 to 80 in JEOL 8030 X-ray diffractmeter. The FT-IR spectra of the samples were recorded as KBr discs in the range 400–1000 cm^{-1} using (FT-IR–Perkin-Elmer, UK, Paragon-500) spectrophotometer. The dc electrical conductivity was recorded as a function of temperature to study the effect of Sn^{4+} substitution using a modified four-probe setup [18].

3. Results and discussion

3.1. Structural properties

X-ray diffraction patterns of the combustion-synthesized $Ni_{1-x}Sn_xFe_2O_4$ ($x = 0.0$, 0.2, 0.4, 0.6, and 0.8) are presented in Figs. 1 and 2(a–d) From Fig. 1 it is observed that the peaks corresponding to the planes (3 1 1), (2 2 0), (4 4 0), confirming the phase formation of pure $NiFe_2O_4$ with a well-defined spinel structure without any impure phase and coinciding with the JCPDS No. 100325. Fig. 2(a)–(d) shows the predominant peaks of $NiFe_2O_4$, NiO and also SnO_2, SnO phases as the tin concentration increases. The intensity of NiO phases shows progressive decrease from Fig. 2(a)–(d), which may be due to dispersion and reducing concentration of nickel. On the other hand the appearance of new intermediate phase of $NiSnO_3$ is also observed. The FCC structure may be assigned to all the compositions from their unmixed $h\,k\,l$ values. The lattice constant a was calculated using the formula $a = d(h^2 + k^2 + l^2)^{1/2}$ and the values are given in Table 1 which are well agreed with the earlier reports [19]. It is seen from the table that the lattice constant remains more or less same for all the compounds due to the proximity of ionic radii of Ni^{2+} and Sn^{4+} cations (0.69 Å). The nanocrystalline nature of the synthesized compounds has been calculated using Debye–Scherror formula of $0.9\lambda/\beta \cos\theta$, where λ is the wavelength of the target Cu Kα 1.5418 Å, β is the full width at half maximum of diffracted (3 1 1) plane. The crystalline sizes are also calculated for other planes, namely (2 2 0), (4 4 0) which led to similar conclusions. The crystalline size was found to vary between 25 and 43 nm as the substitution of Sn^{4+}. The values are given in Table 1. The X-ray density was calculated using the formula $D_{hkl} = 8M/Na^3$, where M is the molecular weight of the sample, N is the Avogadro's number, and a is the lattice parameter of the sample. It is evident from the table

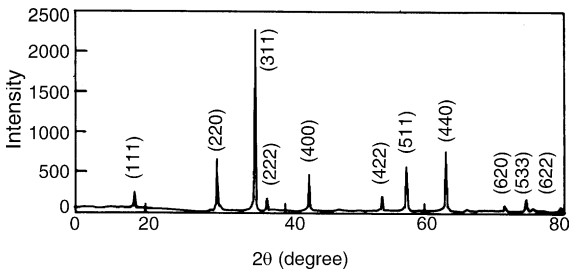

Fig. 1. XRD pattern of $NiFe_2O_4$.

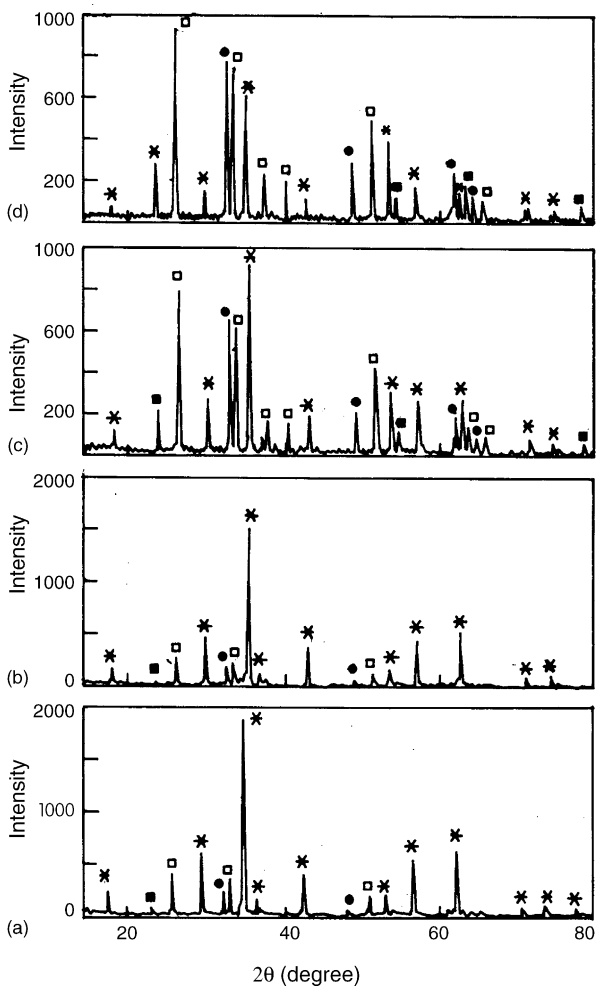

Fig. 2. XRD patterns of $Ni_{1-x}Sn_xFe_2O_4$: (a) $x = 0.2$, (b) $x = 0.4$, (c) $x = 0.6$, and (d) $x = 0.8$, (*) $NiFe_2O_4$, (●) $NiSnO_3$, (□) SnO_2, (■) SnO.

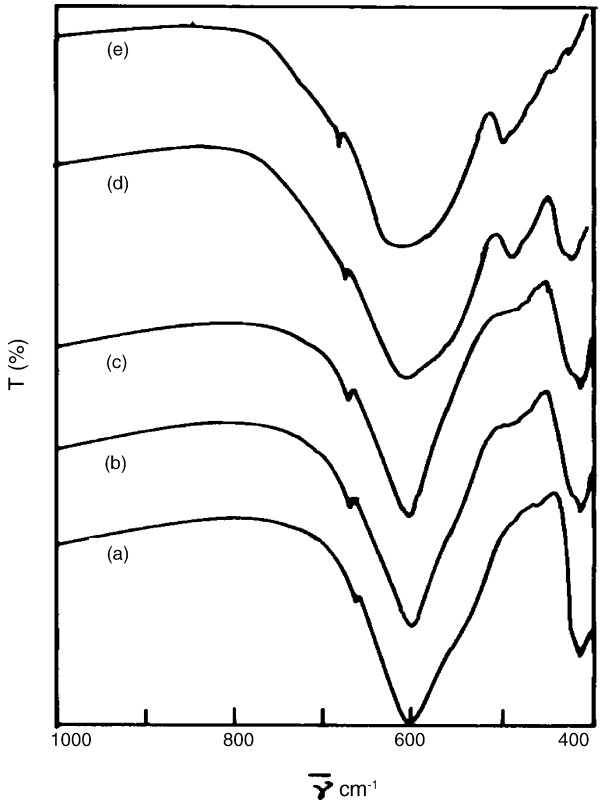

Fig. 3. FT-IR spectra of $Ni_{1-x}Sn_xFe_2O_4$: (a) $x = 0.0$, (b) $x = 0.2$, (c) $x = 0.4$, (d) ($x = 0.6$), and (e) $x = 0.8$.

the X-ray density decreases with increasing concentration of Sn^{4+} substitution.

The IR spectral studies on $NiFe_2O_4$ and substituted ferrite compounds were recorded between 400 and 1000 cm^{-1} and are shown in Fig. 3. The spectra elucidate the position of the ions in the crystal structure and their vibration modes, which represents the various ordering positions on the structural properties of the synthesized compounds. In general the ferrites crystallize in spinel form with the space group $Fd3m - O_h^7$. On the basis of the group theoretical calculations, the spinel ferrites are known to exhibit four fundamentals IR active modes in the vibration spectra, which are high frequency and low frequency bands. In the present study, the absorption bands for the synthesized ferrites are in the expected range. The pure $NiFe_2O_4$ shows absorption bands at 667, 603.1, and 411.8 cm^{-1}. According to Waldron and Hafner [20], the high frequency band υ_1 around 603.1 cm^{-1} is attributed to that of tetrahedral complexes. The variation in the band positions is due to the difference in the Fe^{3+}–O^{2-} distances for the octahedral and tetrahedral complexes. The band values of the $Ni_{1-x}Sn_xFe_2O_4$ (where $x = 0.0$, 0.2, 0.4, 0.6, and 0.8) are given in Table 2. It shows three distinct bands at 600, 412, and 485 cm^{-1}, the band υ_1 around 600 cm^{-1} gets shifted to higher frequency range for all the compositions of Sn^{4+} substitution up to $Sn \leq 0.6$ M. The band υ_2 corresponding to octahedral complexes shows a slight shift towards higher frequencies with diminishing transmittance intensity. A new band υ_3 around 485 cm^{-1} appears on tin substitution which gets more pronounced with the increase in tin concentration. This may be due to the vibration mode corre-

Table 1
XRD parameters

Sample	Lattice constant a_{311} (Å)	FWHM	Crystallite size (nm)	Cell volume (A^3)	X-ray density (g cm^{-3})
$NiFe_2O_4$	8.2340	0.565	25.7	576.63	5.399
$Ni_{0.8}Sn_{0.2}Fe_2O_4$	8.3545	0.565	25.7	583.12	5.299
$Ni_{0.6}Sn_{0.4}Fe_2O_4$	8.3054	0.306	43.0	572.92	5.353
$Ni_{0.4}Sn_{0.6}Fe_2O_4$	8.3413	0.353	41.0	580.36	5.215
$Ni_{0.2}Sn_{0.8}Fe_2O_4$	8.3413	0.400	36.0	580.36	5.205

Table 2
FT-IR parameters

Sites	Bands (cm^{-1})	$Ni_{1-x}Sn_xFe_2O_4$				
		$x = 0.0$	$x = 0.2$	$x = 0.4$	$x = 0.6$	$x = 0.8$
Tetrahedral sites	ν_1^*	603	604	605	605	587
	ν_1^i	667	667	667	667	667
Octahedral sites	ν_2^*	411	412	414	414	
Threshold frequency	ν_{th}	805	825	830	855	850
Threshold energy (eV)	E_{th}	0.0998	0.1023	0.1029	0.1060	0.1054

sponding to Sn^{4+}–O^{2-} complex that increases with increase in Sn concentrations [21]. The spectra for $Sn_{0.8}Ni_{0.2}Fe_2O_4$ show a deviation from other compounds that the υ_1 band corresponding to tetrahedral complexes is broadened and shifted to lower frequency values. The band υ_3 corresponding to the stretching vibration of Sn^{4+}–O^{2-} is shifted to higher value and is more intense than the other substituted compounds. This clearly reveals the maximum concentration of Sn^{4+} ion in the spinel lattice. Mazen et al. have evidenced that the FT-IR spectra as useful tool for calculating the energy associated with the electronic transition and it is calculated using the relation $e_{th} = hf$ [22]. The threshold frequency and energy values are presented in Table 2 shows the general trend of increase.

The diffuse reflectance spectra of the synthesized $Sn_xNi_{1-x}Fe_2O_4$ ($x = 0.0$, 0.2, 0.4, 0.6, and 0.8) samples are shown in Fig. 4. The spectra for the pure $NiFe_2O_4$ compound show the absorbance band around 700 nm, which corresponds to nickel ions in the octahedral sites [23]. The absorbance band around 700 nm shifts towards higher wavelength region as the tin concentration increases. This observation confirms that the Sn^{4+} ion has strong octahedral preference. It is observed from the spectrum for pure $NiFe_2O_4$ that the fundamental absorption edge is found to occur at 566.21 nm where as in the Sn^{4+} substituted compound the values are found at 561.08, 551.11, 543.31, and 576.32 nm, respectively. The band gap values are calculated using the formula $E_a = 1.24/\lambda_{max}$, where λ_{max} is the fundamental absorption edge in μm and is presented Table 3 [24]. The variation in optical band gap shows similar trend as observed in the electrical band gap. This variation may arise from the structural changes and difference in particle sizes.

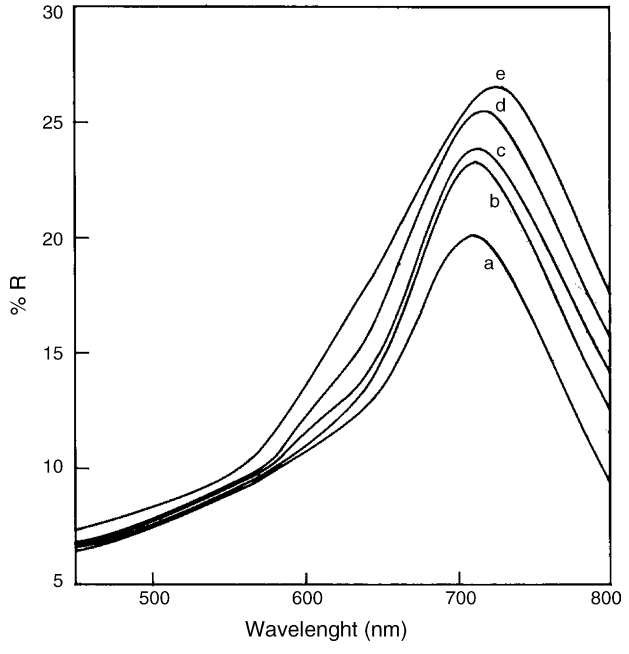

Fig. 4. UV–vis spectra of $Ni_{1-x}Sn_xFe_2O_4$: (a) $x = 0.0$, (b) $x = 0.2$, (c) $x = 0.4$, (d) $x = 0.6$, and (e) $x = 0.8$.

3.2. Electrical properties

The specific conductivity relationship with temperature for a wide range of measuring temperatures from room temperature to 1000 °C continuously is presented in Fig. 5. The results enumerates that the measuring temperature has a positive effect on the conductivity. This may be explained that at high temperatures, the hopping of polarons gets increased which results in high conductivity. Mean while similar observations are made on the specific conductivity values with varying concentrations of tin which shows that the decrease in conductivity up to $x = 0.6$. This may be due to the Sn^{4+} has the strong preference for B-site and has a tendency to replace some Fe^{3+} ions from B-site to A-site. Hence the decrease in number of Fe^{3+} ions in octahedral site decreasing the electronic transition between Fe^{2+} and Fe^{3+} ions, which results in a decrease in conductivity [25]. Since the Ni^{2+} and Sn^{4+} have preferentially occupied strong B-site position the following cation distribution can be assigned to the Sn^{4+} substituted $NiFe_2O_4$.

$$(Fe^{3+})[Ni_{1-x}{}^{2+}Sn_x{}^{4+}Fe^{3+}]O_4$$

Table 3
The optical band gap values

Sample	Band gap (eV)
$NiFe_2O_4$	2.19
$Ni_{0.8}Sn_{0.2}Fe_2O_4$	2.21
$Ni_{0.6}Sn_{0.4}Fe_2O_4$	2.25
$Ni_{0.4}Sn_{0.6}Fe_2O_4$	2.28
$Ni_{0.2}Sn_{0.8}Fe_2O_4$	2.15

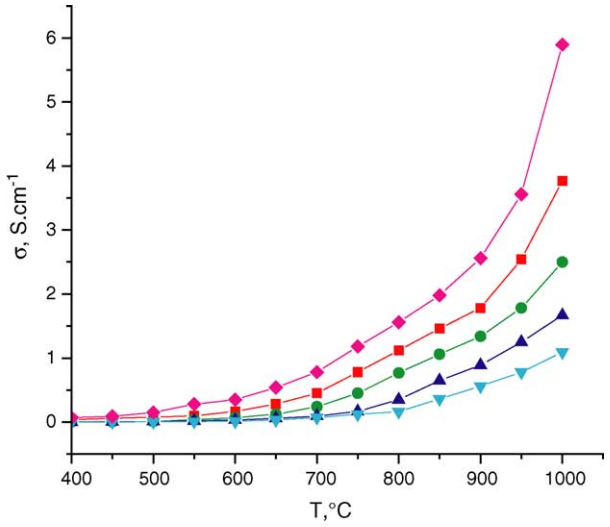

Fig. 5. The dc conductivity vs. temperatures for $Ni_{1-x}Sn_xFe_2O_4$: (■) $x = 0.0$, (●) $x = 0.2$, (▲) $x = 0.4$, (▼) $x = 0.6$, and (♦) $x = 0.8$.

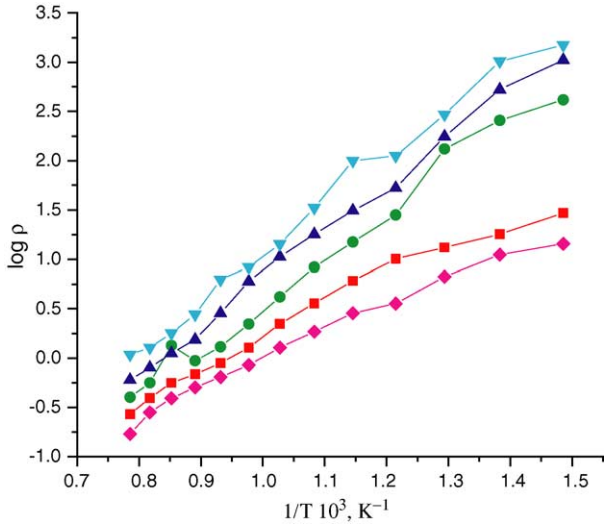

Fig. 6. Arrehenius plot of $Ni_{1-x}Sn_xFe_2O_4$: (■) $x = 0.0$, (●) $x = 0.2$, (▲) $x = 0.4$, (▼) $x = 0.6$, and (♦) $x = 0.8$.

On the other hand, the behavior of $Sn_{0.8}Ni_{0.2}Fe_2O_4$ compound is quite different from other compositions. The conductivity value of the above compound increases abnormally, which is an anomalous behavior. This may be explained that when an ion with variable valency enters the structure, charged vacancies are produced in order to maintain the local charge neutrality. Since Ni^{2+} ions are substituted by Sn^{4+} ions, negative ion vacancies or oxygen vacancies are created which result in high conductivity according to the following mechanism [26].

$$Ni^{2+} \Rightarrow Sn^{4+} + 2e^{-} \quad (5)$$

Hence the following redox reactions may be suggested for the competing conducting mechanism

$$Fe^{2+} \Leftrightarrow Fe^{3+} + e^{-} \quad (6)$$

$$Ni^{3+} \Leftrightarrow Ni^{2+} + e^{+} \quad (7)$$

The activation energies calculated using the Arrehenius equation and from the specific resistivity values are tabulated in Table 4. The Arrehnius plot (Fig. 6) shows three distinct regions with different slopes. Generally, the change in slope is attributed to a change in conduction mechanism. The conduction at low temperature is due to the hopping of electrons between Fe^{2+} and Fe^{3+} ions, whereas at high temperatures, it is due to polaron hopping [27]. The activation energies show direct response to the changes in concentration of tin substitution in nickel ferrite because the substitution could change the energy band structure of the compound.The activation energy for pure nickel ferrite at higher temperature is found to be 0.575 eV, which is in agreement with the earlier reported value [28]. The equation infers that the current carriers are generally electrons originated from Fe^{2+} center, which act as electron donors [29]. At higher temperatures the concentration of Fe^{2+} ions is found to increase along with increased hopping of holes generated from Ni^{3+} to Ni^{2+} ions transition.

The diffusion coefficient of oxygen vacancies in the ferrite was calculated under different temperatures ranging from 400 to 1000 °C with various concentrations of Sn^{4+}, is shown in Fig. 7. This parameter may helpful in the analysis of structural defects in the oxygen sub lattice. The diffusion coefficient of oxygen vacancies is calculated from the relation [30].

$$D = \frac{\sigma k_B T}{Ne^2} \quad (8)$$

where σ is the dc electrical conductivity (S cm^{-1}), N is the number of atoms/m^3, e is the electronic charge, k_B the Boltzmann constant. From the figure, it is evident that the diffu-

Table 4
Activation energies

Sample	Energy gap (eV)					
	Arrehenius plot			Diffusion coefficient		
	Region I	Region II	Region III	Region I	Region II	Region III
$NiFe_2O_4$	0.396	0.793	0.529	0.376	0.853	0.575
$Ni_{0.8}Sn_{0.2}Fe_2O_4$	0.833	0.793	0.634	0.595	1.269	0.674
$Ni_{0.6}Sn_{0.4}Fe_2O_4$	0.872	0.991	0.872	1.031	1.388	0.872
$Ni_{0.4}Sn_{0.6}Fe_2O_4$	0.624	1.16	0.922	0.753	1.309	0.991
$Ni_{0.2}Sn_{0.8}Fe_2O_4$	0.495	0.656	0.515	0.456	0.714	0.495

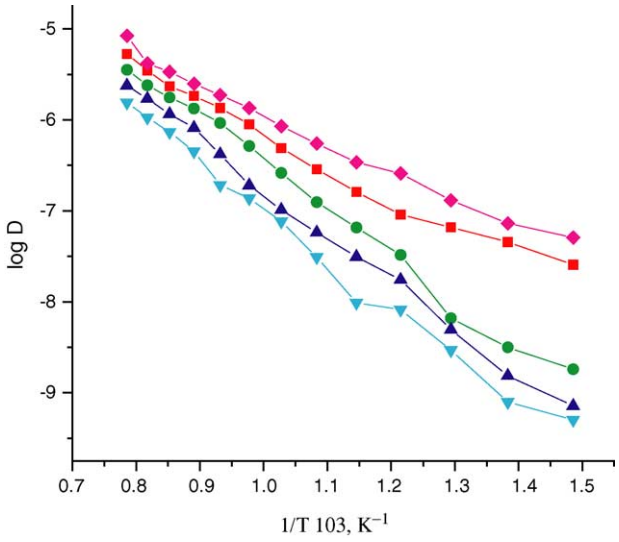

Fig. 7. $\log D$ vs. $1/T \times 10^3\ K^{-1}$ $Ni_{1-x}Sn_xFe_2O_4$: (■) $x = 0.0$, (●) $x = 0.2$, (▲) $x = 0.4$, (▼) $x = 0.6$, and (♦) $x = 0.8$.

sion coefficient increases with increase in temperature. Since, the increase in temperature enhances the mobility of vacancies, which makes more oxygen vacancies to be diffused. The jumping of an atom from its lattice site to the surface, create defects or vacancies; another atom jumps to this vacancy and so on. And in this way oxygen vacancies are distributed throughout the crystal structure. It is also noticed that the diffusion coefficient values vary with the concentration of tin in $NiFe_2O_4$. When the tin ions are substituted in the lattice of $NiFe_2O_4$, the diffusion coefficient values decrease up to a limit of $Sn^{4+} \geq 0.6$ as evident from Fig. 7. This may be corroborated to the occupancy of tin cations in the lattice vacancies. Thus creating a cation vacancy, reducing the diffusion of oxygen vacancies in the sub lattice. Whereas the higher diffusion coefficient values in compounds with higher concentration of tin may be due to the migration of some ferric ions from octahedral to tetrahedral sites and maximum concentration of Sn^{4+} in octahedral sites.

4. Conclusion

Combustion synthesis is confirmed to be one of the simplest and novel methods for preparing new materials. XRD patterns reveal the single-phase compound formation of $NiFe_2O_4$ and poly phases of substituted $NiFe_2O_4$ with nanocrystalline sizes. An intermediate $NiSnO_3$ phase also has been identified from this study during substitution. The stretching and bending vibrational modes of the Ni^{2+}, Sn^{4+}, and Fe^{3+} observed from FT-IR lead to the inference of $NiFe_2O_4$ and substituted compound as an inverse spinel. The band gap values computed from both UV–vis and electrical measurements indicate that the synthesized materials to be semiconductors. The synthesized $NiFe_2O_4$ and substituted compounds are envisaged as suitable anode material on the basis of their evaluated electrical and structural characteristics.

Acknowledgements

The authors express their gratitude to the Director, CECRI, Staff of Electropyrometallurgy Division and Characterization laboratory for their kind help.

References

[1] L. Sathyanarayana, K. Madusudhan Reddy, S.V. Manorama, Mater. Chem. Phys. 82 (2003) 21.
[2] R. Alcantra, M. Jaraba, P. Lavela, J.L. Tirado, J.C. Jumas, J. Oliver, Electrochem. Commun. 5 (2003) 16.
[3] E. Olsen, J. Thonstad, J. Appl. Electrochem. 29 (1999) 293.
[4] L. John Berchmans, R. Kalai Selvan, C.O. Augustin, Mater. Lett. 58 (2004) 1928.
[5] Q. Yitai, X. Yi, L. Jing, C. Zuyao, Y. Li, Mater. Sci. Eng. B 34 (1995) 11.
[6] V.K. Sankaranarayanan, C. SreeKumar, Curr. Appl. Phys. 3 (2003) 205.
[7] P. Yadoji, R. Peelamedu, D. Agrawal, R. Roy, Mater. Sci. Eng. B 98 (2003) 269.
[8] B.K. Labde, M.C. Cable, N.R. Sham Kumar, Mater. Lett. 57 (2003) 1651.
[9] Z. Yue, L. Li, J. Zhou, H. Zhang, Z. Gui, Mater. Sci. Eng. B 64 (1999) 68.
[10] D. Ravinder, S. Srinivasa Rao, P. Shalini, Mater. Lett. 57 (2003) 4040.
[11] Giang-Min. Kui, Jian-bao, Y.C. Han, Mater. Chem. Phys. 74 (2002) 340.
[12] M.Z. Said, Mater. Lett. 34 (1998) 305.
[13] L. John Berchmans, R. Kalai Selvan, P.N. Selva Kumar, C.O. Augustin, J. Magn. Magn. Mater. 279 (2004) 103.
[14] D.-C. Boe, S. woo Kim, H.-W. Lee, K.S. Han, Mater. Lett. 57 (2003) 1997.
[15] J.S. Baijal, D. Kothari, S.P.C. Prakash, Solid State Commun. 69 (1989) 277.
[16] D. Siegel, J. Mater. Chem. 7 (1999) 1297.
[17] R. Kalai Selvan, C.O. Augustin, L. John Berchmans, R. Saraswathi, Mater. Res. Bull. 38 (2003) 41.
[18] C.O. Augustin, D. Prabakaran, L.K. Srinivasan, J. Mater. Sci. Lett. 12 (1993) 383.
[19] A.A. Bandit, S.S. More, R.G. Dovik, K.N. Jadov, Bull. Mater. Sci. 26 (2003) 517.
[20] R.D. Waldron, Phys. Rev. 99 (1955) 1727.
[21] O.S. Josyulu, J. Sobanadri, Phys. Status Solidi 65 (1981) 131.
[22] S.A. Mazen, Mater. Chem. Phys. 62 (2000) 131.
[23] P. Jeevanandam, Yu. Kotypin, A. Gedanken, Mater. Sci. Eng. B 90 (2002) 125.
[24] S. Esther Dali, M.J. Chockalingam, Mater. Chem. Phys. 70 (2001) 73.
[25] M. Singh, S.P. Sud, Mater. Sci. Eng. B 83 (1998) 180.
[26] J.Y. Lee, H.S. Kee, K.S. Ahm, Mater. Chem. Phys. 52 (1998) 267.
[27] D. Ravinder, B. Ravikumar, Mater. Lett. 57 (2003) 1738.
[28] B. Lduey, N.B. Singh, J.N. Srivastava, A.K. Dha, Ind. J. Chem. 40A (2001) 841.
[29] M. Rosenberg, P. Nicolous, I. Bunget, Phys. Status Solidi 13 (1966) 521.
[30] O.M. Hameda, M.E.L. Saadawan, J. Magn. Magn. Mater. 256 (2003) 63.